Multipole decompositions for directional light scattering

Andrey B. Evlyukhin[1,2,*] and Boris N. Chichkov[1,2,3]
[1]*Institute of Quantum Optics, Leibniz Universität Hannover, Welfengarten strasse 1, 30167 Hannover, Germany*
[2]*Laboratory of Nano and Quantum Engineering, Leibniz Universität Hannover, Hannover, Germany*
[3]*Lebedev Physical Institute, Leninsky Prospect 53, 119333 Moscow, Russia*

(Received 15 June 2019; revised manuscript received 29 August 2019; published 12 September 2019)

Applications of the multipole decomposition method for investigations of directional light scattering by a single nanoparticle and nanoparticle structures located in a finite spatial region are discussed. It is shown that, even in the case of relatively large scatterers, the multipole decomposition obtained in the long-wavelength approximation (LWA) may provide much better convergence than the multipole decomposition with the exact multipoles obtained from the spherical harmonics expansion. For an explanation of this seeming paradox, we derive in real space the exact multipole decomposition based on the spherical harmonics, presenting exact expressions for multipoles up to the electric 16-pole. Results obtained with the exact and approximate multipole expressions are discussed and compared. It is shown that for shape-anisotropic finite-size scatterers with different geometrical dimensions (like plates, rods, disks, rings, etc.), the required number of approximate multipoles providing accurate results may be much smaller than the required number of exact multipoles. For applicability of the LWA multipole decomposition, the only important parameter is the small ratio of the scatter size (its projection) in the scattering direction to the light wavelength. If this condition is fulfilled, the multipole decomposition with a small number of LWA multipoles is simpler than that based on the exact multipoles.

DOI: 10.1103/PhysRevB.100.125415

I. INTRODUCTION

The multipole analysis of electromagnetic fields radiated (or scattered) by an object with confined charges and currents provides important information about the spatial distribution of the radiated (or scattered) waves and about interaction of external radiation with this object. The main advantage of this approach lies in the replacement of complex field distributions by the superposition of fields generated by point sources, called multipole moments, corresponding to the object's charge and current distributions [1].

The number and type of multipole moments which effectively describe the generated fields are determined by the size and shape of the regions containing electric charges and currents. It is well known that if the wavelength of generated fields is much larger than the object size, only the lowest-order multipoles (such as dipoles or quadrupoles) provide contributions to the generated fields. In this case the multipole moments are determined to be the first low-order coefficients of Taylor expansion for the retarded potentials of the electromagnetic field generated by oscillating electric charges and currents [1,2]. Frequently, these multipoles (obtained in the long-wavelength approximation) are used as ordinary multipole moments [3,4] for investigations of electromagnetic scattering by nanoparticles and finite-size nanostructures [5–8]. With the growing scatterer sizes, the number of multipole terms, which must be taken into account for correct approximation of the scattered field, increases rapidly. These multipole terms may include ordinary multipole moments and the so-called mean-square radii [4,9–11] or high-order toroidal moments [12].

Another alternative multipole approach to electromagnetic scattering by finite-size objects is based on the multipole expansion of the scattered field using spherical harmonics [1]. In this case the multipole moments are the coefficients of corresponding expansion which can be calculated from the distribution of generated electric field on any spherical surface enclosing the finite-size scattering object [13]. By expressing the generated field on the spherical surface through the source currents and charges, the connection of multipole moments with the current and charge distributions can be obtained [1,13]. In this approach, there are no limitations on the source sizes and radiated wavelengths, as has been shown in the Mie theory for spherical particles [14]. A comprehensive discussion of the topics related to different multipole decompositions for applications in nanophotonics can be found in a recent review [15]. On the basis of previous publications [16,17], where new *exact* analytical expressions for the multipole moments of a localized electric current density distribution were derived, direct correspondence of different multipole decompositions was demonstrated. Moreover, it has been shown that the multipole moments derived in the long-wavelength approximation (LWA) [12] can be directly obtained from the exact multipoles using a simple limiting transition to large wavelengths [16].

Due to the relative simplicity of the derived exact expressions for multipole moments [15], one can expect that they will outweigh and potentially completely replace the LWA multipole moments in the analysis of light-scattering problems. However, as will be shown in this paper, the application of LWA multipoles, obtained from the Taylor expansion of

*a.b.evlyukhin@daad-alumni.de

the retarded potentials, may be more advantageous and simple for investigations of directional scattering, even for large shape-anisotropic objects. The LWA multipoles can be useful for multipole decomposition of the extinction cross sections calculated from the optical theorem [18] because in this case only the information about forward scattering is required. In Sec. II, direct derivations of the exact multipole moments in real space are performed. In Sec. III, we analyze applications of the exact and LWA multipole moments for investigations of directional light scattering. Examples demonstrating the advantages of the LWA multipole applications are presented in Sec. IV. A summary of the main results is given in Sec. V.

II. MULTIPOLE DECOMPOSITIONS

In the framework of Green's tensor formalism, scattering of a monochromatic electric field with time dependence $\exp(-i\omega t)$ (where ω is the field angular frequency) outside the finite-size scatterer is determined by [19,20]

$$\mathbf{E}(\mathbf{r}) = \omega^2\mu_0 \int_{V_s} \hat{G}(\mathbf{r},\mathbf{r}')\mathbf{P}(\mathbf{r}')d\mathbf{r}', \tag{1}$$

or

$$\mathbf{E}(\mathbf{r}) = i\omega\mu_0 \int_{V_s} \hat{G}(\mathbf{r},\mathbf{r}')\,\mathbf{j}(\mathbf{r}')d\mathbf{r}', \tag{2}$$

where $\mathbf{j}(\mathbf{r}')$ and $\mathbf{P}(\mathbf{r}')$ are the induced electric current density and electric polarization, respectively, so that $\mathbf{j}(\mathbf{r}') = -i\omega\mathbf{P}(\mathbf{r}')$, $\mathbf{r}$ is the radius vector of the observation point, V_s is the scatterer volume, and μ_0 is the vacuum magnetic permeability. We assume that the origin of the Cartesian coordinate system is located in the region occupied by the scatterer. In the far-wave approximation, where $|\mathbf{r}| = r \gg 1/k_d$, $r \gg |\mathbf{r}'| = r'$ (for any $\mathbf{r}'$ from the volume V_s), and k_d is the wave number in the surrounding medium, the Green's tensor of the homogeneous infinite medium with the dielectric constant ε_d is given by [21]

$$\hat{G}_0^{FF}(\mathbf{r},\mathbf{r}') = \frac{e^{ik_d r}}{4\pi r}(\hat{U} - \mathbf{nn})e^{-ik_d(\mathbf{n}\cdot\mathbf{r}')}, \tag{3}$$

where $\mathbf{nn}$ is the tensor product of the unit vector $\mathbf{n} = \mathbf{r}/r$ of the observation point defining the scattering direction and $\hat{U}$ is the 3×3 unit tensor. The relation between r' and $1/k_d$ can be arbitrary, including the case of $k_d r' > 1$; that is, there are no limitations on the biggest scatterer dimension D (however, for the observation point the condition $r \gg D$ should be fulfilled). Thus, the radiated (scattered) electric field in the direction $\mathbf{n}$ is [1]

$$\mathbf{E}_\mathbf{n}(\mathbf{r}) = i\omega\mu_0 \frac{e^{ik_d r}}{4\pi r}(\hat{U} - \mathbf{nn}) \int_{V_s} e^{-ik_d(\mathbf{n}\cdot\mathbf{r}')}\,\mathbf{j}(\mathbf{r}')d\mathbf{r}'. \tag{4}$$

Using Eq. (4), multipole decompositions of scattered waves can be obtained by several approaches, but they are always related to the exponential factor $\exp[-ik_d(\mathbf{n}\cdot\mathbf{r}')]$: (i) it is possible to expand this exponential factor in a Taylor series around a point with the radius vector $\mathbf{r}_0$ located in the volume V_s [1]; (ii) it is possible to write the electric current density as

$$\mathbf{j}(\mathbf{r}') = \int_{V_s} \mathbf{j}(\mathbf{r})\delta(\mathbf{r}' - \mathbf{r})d\mathbf{r}$$

and then to expand delta function $\delta(\mathbf{r}' - \mathbf{r})$ in a Taylor series around a point $\mathbf{r}_0$ [18,21], smf (iii) it is possible to expand the exponential factor $\exp[-ik_d(\mathbf{n}\cdot\mathbf{r}')]$ in spherical harmonics [1]. The first two approaches are equivalent to each other and provide multipoles in the LWA [16]. Since the Taylor expansion of the exponential factor is convergent for any finite value of its argument, it can be applied for multipole decomposition of the scattered field by finite-size scatterers with arbitrary dimensions [12].

The third approach is applied in this paper for the derivation of exact spherical multipoles using the following notations: the signs $\times$ and $\cdot$ denote vector and scalar products; the tensor product of vectors $\mathbf{a}$, $\mathbf{b}$, and $\mathbf{c}$ is written $\mathbf{abc}$ and represents a third-rank tensor.

A. Long-wavelength approximation

For further discussions we recall that if $k_d r' \ll 1$ for any $\mathbf{r}'$ from the volume V_s, the Taylor expansion of the exponential factor under the integral in Eq. (4) can be limited by several low-order terms, and the well-known LWA multipole decomposition of $\mathbf{E}_\mathbf{n}$ can be obtained [5,18],

$$\begin{aligned}\mathbf{E}_\mathbf{n}(\mathbf{r}) \simeq \frac{k_0^2 e^{ik_d r}}{4\pi\varepsilon_0 r}\Bigg\{&\left[\mathbf{n}\times\left[\left(\mathbf{p} + \frac{ik_d}{v_d}\mathbf{T}\right)\times\mathbf{n}\right]\right] + \frac{1}{v_d}[\mathbf{m}\times\mathbf{n}] \\ &+ \frac{ik_d}{6}[\mathbf{n}\times[\mathbf{n}\times\hat{Q}\mathbf{n}]] + \frac{ik_d}{2v_d}[\mathbf{n}\times(\hat{M}\mathbf{n})] \\ &+ \frac{k_d^2}{6}[\mathbf{n}\times[\mathbf{n}\times\hat{O}(\mathbf{nn})]]\Bigg\},\end{aligned} \tag{5}$$

where $k_0 = \omega\sqrt{\mu_0\varepsilon_0}$ is the wave number in vacuum, ε_0 is the vacuum permittivity, v_d is the speed of light in the surrounding medium with ε_d, and the Cartesian multipoles (the electric dipole $\mathbf{p}$, toroidal dipole $\mathbf{T}$, magnetic dipole $\mathbf{m}$, electric quadrupole tensor $\hat{Q}$, magnetic quadrupole tensor $\hat{M}$, and electric octupole tensor $\hat{O}$) are presented in the long-wavelength approximation. These multipole tensors are used in the traceless and symmetrical (irreducible) representations. Analytical expressions determining the multipole moments of different orders can be found in [12,18]. Note that the definition of the traceless electric quadrupole moment from Ref. [18] differs from the quadrupole moment considered in Ref. [12] by a factor of 3. For transition from Eq. (4) to (5), we used the identity

$$(\hat{U} - \mathbf{nn})\mathbf{b} = [\mathbf{n}\times[\mathbf{b}\times\mathbf{n}]],$$

where $\mathbf{b}$ is an arbitrary vector. The origin of the Cartesian coordinate system is chosen at the multipole location point.

B. The exact spherical multipole decomposition

In addition to previous publications [16,17], exact spherical multipole decomposition can be obtained directly from Eq. (4) in the Cartesian basis using plane wave representation in spherical harmonics [1],

$$e^{-ik_d(\mathbf{n}\cdot\mathbf{r}')} = 4\pi\sum_{l=0}^{\infty}\sum_{m=-l}^{l}(-i)^l j_l(k_d r')Y_{lm}^*(\theta,\varphi)Y_{lm}(\theta',\varphi'), \tag{6}$$

where $j_l(k_d r')$ is the lth order spherical Bessel function, $Y_{lm}(\theta, \varphi)$ is the scalar spherical harmonics, θ and φ (θ' and φ') are the polar and azimuthal angles of $\mathbf{n}$ ($\mathbf{r}'$) in the spherical coordinate system, and the asterisk (*) denotes the complex conjugation. Inserting Eq. (6) into (4), one can write

$$\begin{aligned}\mathbf{E_n}(\mathbf{r}) &= i\omega\mu_0 \frac{e^{ik_d r}}{4\pi r}(\hat{U} - \mathbf{nn}) \\ &\times \sum_{l,m} 4\pi(-i)^l Y^*_{lm}(\theta,\varphi)\int_{V_s} j_l(k_d r')Y_{lm}(\theta',\varphi')\mathbf{j}(\mathbf{r}')d\mathbf{r}' \\ &= i\omega\mu_0 \frac{e^{ik_d r}}{4\pi r}(\hat{U} - \mathbf{nn}) \\ &\times \sum_{l=0}^{\infty}(-i)^l(2l+1)\int_{V_s} j_l(k_d r')P_l(\cos\gamma)\mathbf{j}(\mathbf{r}')d\mathbf{r}' \\ &= i\omega\mu_0 \frac{e^{ik_d r}}{4\pi r}(\hat{U} - \mathbf{nn})\sum_{l=0}^{\infty}\mathbf{S}_l, \end{aligned} \tag{7}$$

where P_l is the l-order Legendre polynomial. Above, the additional theorem for spherical harmonics was used [1]:

$$P_l(\cos\gamma) = \frac{4\pi}{2l+1}\sum_{m=-l}^{l} Y^*_{lm}(\theta',\varphi')Y_{lm}(\theta,\varphi), \tag{8}$$

where γ is the angle between two unit vectors $\mathbf{n} = \mathbf{r}/r = (\sin\theta\cos\varphi, \sin\theta\sin\varphi, \cos\theta)$ and $\mathbf{n}' = \mathbf{r}'/r' = (\sin\theta'\cos\varphi', \sin\theta'\sin\varphi', \cos\theta')$, so that $\cos\gamma = (\mathbf{n}\cdot\mathbf{n}') = \cos\theta\cos\theta' + \sin\theta\sin\theta'\cos(\varphi - \varphi')$. The required information about the Legendre polynomials can be found elsewhere [22].

We consider several low-order terms of $\mathbf{S}_l$ in the sum of Eq. (7). For $l = 0$, $P_0(\cos\gamma) = 1$, we have

$$\mathbf{S}_0 = \int_{V_s} j_0(k_d r')\mathbf{j}(\mathbf{r}')d\mathbf{r}'. \tag{9}$$

For $l = 1$, $P_1(\cos\gamma) = (\mathbf{n}\cdot\mathbf{r}'/r')$, we get

$$\begin{aligned}\mathbf{S}_1 &= -3ik_d\int_{V_s}\frac{j_1(k_d r')}{k_d r'}(\mathbf{n}\cdot\mathbf{r}')\mathbf{j}(\mathbf{r}')d\mathbf{r}' \\ &= \frac{3}{2}ik_d\int_{V_s}\frac{j_1(k_d r')}{k_d r'}[\mathbf{n}\times[\mathbf{r}'\times\mathbf{j}]]d\mathbf{r}' \\ &- \frac{ik_d}{2}\int_{V_s}\frac{j_1(k_d r')}{k_d r'}[3(\mathbf{r}'\mathbf{j} + \mathbf{j}\mathbf{r}') - 2(\mathbf{r}'\cdot\mathbf{j})\hat{U}]\mathbf{n}d\mathbf{r}' \\ &- ik_d\int_{V_s}\frac{j_1(k_d r')}{k_d r'}(\mathbf{r}'\cdot\mathbf{j})\mathbf{n}d\mathbf{r}'. \end{aligned} \tag{10}$$

Above, the following transformation was used:

$$\begin{aligned}(\mathbf{n}\cdot\mathbf{r}')\mathbf{j} = (\mathbf{j}\mathbf{r}')\mathbf{n} &= -\frac{1}{2}[\mathbf{n}\times[\mathbf{r}'\times\mathbf{j}]] \\ &+ \frac{1}{6}[3(\mathbf{r}'\mathbf{j} + \mathbf{j}\mathbf{r}') - 2(\mathbf{r}'\cdot\mathbf{j})\hat{U}]\mathbf{n} \\ &+ \frac{1}{3}(\mathbf{r}'\cdot\mathbf{j})\mathbf{n}. \end{aligned} \tag{11}$$

For $l = 2$, $P_2(\cos\gamma) = (3[\mathbf{n}\cdot\mathbf{r}'/r']^2 - 1)/2$, we obtain

$$\begin{aligned}\mathbf{S}_2 &= -\frac{5}{2}k_d^2\int_{V_s}\frac{j_2(k_d r')}{k_d^2 r'^2}[3(\mathbf{n}\cdot\mathbf{r}')^2 - r'^2]\mathbf{j}(\mathbf{r}')d\mathbf{r}' \\ &= -\frac{5}{2}k_d^2\int_{V_s}\frac{j_2(k_d r')}{k_d^2 r'^2}(\mathbf{j}\mathbf{r}'\mathbf{r}' + \mathbf{r}'\mathbf{j}\mathbf{r}' + \mathbf{r}'\mathbf{r}'\mathbf{j} - \hat{A})(\mathbf{nn})d\mathbf{r}' \\ &+ \frac{5}{2}k_d^2\int_{V_s}\frac{j_2(k_d r')}{k_d^2 r'^2}[\mathbf{n}\times\big([\mathbf{r}'\times\mathbf{j}]\mathbf{r}' + \mathbf{r}'[\mathbf{r}'\times\mathbf{j}]\big)\mathbf{n}]d\mathbf{r}' \\ &+ \frac{1}{2}k_d^2\int_{V_s}\frac{j_2(k_d r')}{k_d^2 r'^2}[3(\mathbf{r}'\cdot\mathbf{j})\mathbf{r}' - r'^2\mathbf{j}]d\mathbf{r}' \\ &- \frac{5}{2}k_d^2\mathbf{n}\int_{V_s}\frac{j_2(k_d r')}{k_d^2 r'^2}[[\mathbf{r}'(\mathbf{r}'\cdot\mathbf{j}) - r'^2\mathbf{j}]\cdot\mathbf{n}]d\mathbf{r}' \\ &- 5k_d^2\mathbf{n}\int_{V_s}\frac{j_2(k_d r')}{k_d^2 r'^2}(\mathbf{n}\cdot\mathbf{V})d\mathbf{r}', \end{aligned} \tag{12}$$

where

$$A_{\beta\gamma\tau} = \delta_{\beta\gamma}V_\tau + \delta_{\beta\tau}V_\gamma + \delta_{\gamma\tau}V_\beta, \tag{13}$$

$\beta = x, y, z$, $\gamma = x, y, z$, $\tau = x, y, z$, and $\delta_{\beta\gamma}$ is the Kronecker delta,

$$\mathbf{V} = \frac{1}{5}[2(\mathbf{r}'\cdot\mathbf{j})\mathbf{r}' + r'^2\mathbf{j}]. \tag{14}$$

Above, the following tensor identity was used:

$$(\mathbf{n}\cdot\mathbf{r}')^2\mathbf{j} = (\mathbf{j}\mathbf{r}'\mathbf{r}')(\mathbf{nn}), \tag{15}$$

and then procedures of symmetrization and detracing to the tensor $\mathbf{j}\mathbf{r}'\mathbf{r}'$ were applied (details can be found in supplementary materials in Ref. [12]).

For $l = 3$, $P_3(\cos\gamma) = (5[\mathbf{n}\cdot\mathbf{r}'/r']^3 - 3[\mathbf{n}\cdot\mathbf{r}'/r'])/2$, we have

$$\begin{aligned}\mathbf{S}_3 &= \frac{7}{2}ik_d^3\int_{V_s}\frac{j_3(k_d r')}{k_d^3 r'^3}[5(\mathbf{n}\cdot\mathbf{r}')^3 - 3(\mathbf{n}\cdot\mathbf{r}')r'^2]\mathbf{j}(\mathbf{r}')d\mathbf{r}' \\ &= \frac{105}{24}ik_d^3\int_{V_s}\frac{j_3(k_d r')}{k_d^3 r'^3}(\mathbf{j}\mathbf{r}'\mathbf{r}'\mathbf{r}' + \mathbf{r}'\mathbf{j}\mathbf{r}'\mathbf{r}' \\ &+ \mathbf{r}'\mathbf{r}'\mathbf{j}\mathbf{r}' + \mathbf{r}'\mathbf{r}'\mathbf{r}'\mathbf{j} - \hat{B})(\mathbf{nnn})d\mathbf{r}' \\ &- \frac{105}{6\times 4}ik_d^3\int_{V_s}\frac{j_3(k_d r')}{k_d^3 r'^3}[\mathbf{n}\times([\mathbf{r}'\times\mathbf{j}]\mathbf{r}'\mathbf{r}' \\ &+ \mathbf{r}'[\mathbf{r}'\times\mathbf{j}]\mathbf{r}' + \mathbf{r}'\mathbf{r}'[\mathbf{r}'\times\mathbf{j}] - \hat{A}')\mathbf{nn}]d\mathbf{r}' \\ &+ ik_d^3\int_{V_s}\frac{j_3(k_d r')}{k_d^3 r'^3}[r'^2(\mathbf{j}\mathbf{r}' + \mathbf{r}'\mathbf{j}) - 5(\mathbf{j}\cdot\mathbf{r}')\mathbf{r}'\mathbf{r}' \\ &+ (\mathbf{j}\cdot\mathbf{r}')r'^2\hat{U}]\mathbf{n}d\mathbf{r}' \\ &+ \frac{15}{8}ik_d^3\int_{V_s}\frac{j_3(k_d r')}{k_d^3 r'^3}(\hat{C}:\mathbf{nn})\mathbf{n}d\mathbf{r}' \\ &- \frac{35}{4}ik_d^3\int_{V_s}\frac{j_3(k_d r')}{k_d^3 r'^3}\Big\{\mathbf{n}\cdot[(\mathbf{r}'\cdot\mathbf{j})\mathbf{r}'\mathbf{r}' \\ &- \frac{1}{2}r'^2(\mathbf{r}'\mathbf{j} + \mathbf{j}\mathbf{r}')]\mathbf{n}\Big\}\mathbf{n}d\mathbf{r}', \end{aligned} \tag{16}$$

where

$$A'_{\beta\gamma\tau} = \delta_{\beta\gamma}V'_\tau + \delta_{\beta\tau}V'_\gamma + \delta_{\gamma\tau}V'_\beta, \tag{17}$$

$\beta = x, y, z$, $\gamma = x, y, z$, $\tau = x, y, z$, and $\delta_{\beta\gamma}$ is the Kronecker delta.

$$\mathbf{V}' = \frac{1}{5} r'^2 [\mathbf{r}' \times \mathbf{j}], \tag{18}$$

$$\begin{aligned} B_{\alpha\beta\gamma\tau} = {} & \frac{1}{7}(\delta_{\alpha\beta}C_{\gamma\tau} + \delta_{\alpha\gamma}C_{\beta\tau} + \delta_{\alpha\tau}C_{\beta\gamma} \\ & + \delta_{\beta\tau}C_{\alpha\gamma} + \delta_{\beta\gamma}C_{\alpha\tau} + \delta_{\gamma\tau}C_{\beta\alpha}) \\ & + \frac{4}{15}(\mathbf{j}\cdot\mathbf{r}')r'^2(\delta_{\alpha\beta}\delta_{\gamma\tau} + \delta_{\alpha\gamma}\delta_{\beta\tau} + \delta_{\alpha\tau}\delta_{\beta\gamma}), \end{aligned} \tag{19}$$

and

$$\hat{C} = 2(\mathbf{j}\cdot\mathbf{r}')\mathbf{r}'\mathbf{r}' + r'^2(\mathbf{j}\mathbf{r}' + \mathbf{r}'\mathbf{j}) - \frac{4}{3}(\mathbf{j}\cdot\mathbf{r}')r'^2\hat{U}.$$

In order to get Eq. (16), we used the following tensor identity:

$$(\mathbf{n}\cdot\mathbf{r}')^3\mathbf{j} = (\mathbf{j}\mathbf{r}'\mathbf{r}'\mathbf{r}')(\mathbf{nnn}) \tag{20}$$

and then again applied the procedures of symmetrization and detracing to the tensor $\mathbf{j}\mathbf{r}'\mathbf{r}'\mathbf{r}'$ [12].

Introducing multipole moments similar to [16]

$$\mathbf{p}_0 = \frac{i}{\omega}\int_{V_s} j_0(k_d r')\mathbf{j}(\mathbf{r}')d\mathbf{r}', \tag{21}$$

$$\mathbf{m}_1 = \frac{3}{2}\int_{V_s} \frac{j_1(k_d r')}{k_d r'}[\mathbf{r}' \times \mathbf{j}]d\mathbf{r}', \tag{22}$$

$$\hat{Q}_1 = \frac{3i}{\omega}\int_{V_s} \frac{j_1(k_d r')}{k_d r'}[3(\mathbf{r}'\mathbf{j} + \mathbf{j}\mathbf{r}') - 2(\mathbf{r}'\cdot\mathbf{j})\hat{U}]d\mathbf{r}', \tag{23}$$

$$\hat{M}_2 = 5\int_{V_s} \frac{j_2(k_d r')}{(k_d r')^2}([\mathbf{r}' \times \mathbf{j}]\mathbf{r}' + \mathbf{r}'[\mathbf{r}' \times \mathbf{j}])d\mathbf{r}', \tag{24}$$

$$\mathbf{T}_2 = \frac{ik_d^2}{\omega 2}\int_{V_s} \frac{j_2(k_d r')}{(k_d r')^2}[3(\mathbf{r}'\cdot\mathbf{j})\mathbf{r}' - r'^2\mathbf{j}]d\mathbf{r}', \tag{25}$$

$$\hat{O}_2^{(e)} = \frac{15i}{\omega}\int_{V_s} \frac{j_2(k_d r')}{(k_d r')^2}(\mathbf{j}\mathbf{r}'\mathbf{r}' + \mathbf{r}'\mathbf{j}\mathbf{r}' + \mathbf{r}'\mathbf{r}'\mathbf{j} - \hat{A})d\mathbf{r}', \tag{26}$$

$$\begin{aligned} \hat{Q}_3 = {} & \frac{6ik_d^2}{\omega}\int_{V_s} \frac{j_3(k_d r')}{k_d^3 r'^3}[5(\mathbf{j}\cdot\mathbf{r}')\mathbf{r}'\mathbf{r}' - r'^2(\mathbf{j}\mathbf{r}' + \mathbf{r}'\mathbf{j}) \\ & - (\mathbf{j}\cdot\mathbf{r}')r'^2\hat{U}]d\mathbf{r}', \end{aligned} \tag{27}$$

$$\begin{aligned} \hat{O}_3^{(m)} = {} & \frac{105}{4}\int_{V_s} \frac{j_3(k_d r')}{k_d^3 r'^3}([\mathbf{r}' \times \mathbf{j}]\mathbf{r}'\mathbf{r}' + \mathbf{r}'[\mathbf{r}' \times \mathbf{j}]\mathbf{r}' \\ & + \mathbf{r}'\mathbf{r}'[\mathbf{r}' \times \mathbf{j}] - \hat{A}')d\mathbf{r}', \end{aligned} \tag{28}$$

$$\begin{aligned} \hat{S}_3^{(e)} = {} & \frac{105i}{\omega}\int_{V_s} \frac{j_3(k_d r')}{k_d^3 r'^3}(\mathbf{j}\mathbf{r}'\mathbf{r}'\mathbf{r}' + \mathbf{r}'\mathbf{j}\mathbf{r}'\mathbf{r}' \\ & + \mathbf{r}'\mathbf{r}'\mathbf{j}\mathbf{r}' + \mathbf{r}'\mathbf{r}'\mathbf{r}'\mathbf{j} - \hat{B})d\mathbf{r}', \end{aligned} \tag{29}$$

the above $\mathbf{S}_l$ terms can be rewritten as

$$\mathbf{S}_0 = -i\omega\mathbf{p}_0, \tag{30}$$

$$\mathbf{S}_1 = ik_d[\mathbf{n} \times \mathbf{m}_1] - \frac{\omega k_d}{6}(\hat{Q}_1\mathbf{n}) - ik_d L_1\mathbf{n}, \tag{31}$$

$$\begin{aligned} \mathbf{S}_2 = {} & \frac{i\omega k_d^2}{6}(\hat{O}_2^{(e)}\mathbf{nn}) + \frac{k_d^2}{2}[\mathbf{n} \times (\hat{M}_2\mathbf{n})] - i\omega\mathbf{T}_2 \\ & + 3i\omega(\mathbf{T}_2\cdot\mathbf{n})\mathbf{n}, \end{aligned} \tag{32}$$

$$\begin{aligned} \mathbf{S}_3 = {} & -\frac{ik_d^3}{6}[\mathbf{n} \times (\hat{O}_3^{(m)}\mathbf{nn})] - \frac{\omega k_d}{6}(\hat{Q}_3\mathbf{n}) \\ & + \frac{\omega k_d^3}{24}(\hat{S}_3^{(e)}\mathbf{nnn}) + \frac{5ik_d^3}{4}(\mathbf{n}\cdot(\hat{L}_3\mathbf{n}))\mathbf{n}, \end{aligned} \tag{33}$$

where the scalar term with

$$L_1 = \int_{V_s} \frac{j_1(k_d r')}{k_d r'}(\mathbf{r}'\cdot\mathbf{j})d\mathbf{r}'$$

and the tensor term with

$$\hat{L}_3 = \int_{V_s} \frac{j_3(k_d r')}{k_d^3 r'^3}[5r'^2(\mathbf{j}\mathbf{r}' + \mathbf{r}'\mathbf{j}) - 4(\mathbf{j}\cdot\mathbf{r}')\mathbf{r}'\mathbf{r}' - 2(\mathbf{j}\cdot\mathbf{r}')r'^2\hat{U}]d\mathbf{r}'$$

correspond to nonradiating contributions.

For the scattered electric field from Eq. (7), we obtain

$$\begin{aligned} \mathbf{E}_\mathbf{n}(\mathbf{r}) = {} & i\omega\mu_0\frac{e^{ik_d r}}{4\pi r}(\hat{U} - \mathbf{nn})(\mathbf{S}_0 + \mathbf{S}_1 + \mathbf{S}_2 + \mathbf{S}_3 + \cdots) \\ \simeq {} & k_0^2\frac{e^{ik_d r}}{\varepsilon_0 4\pi r}\Bigg([\mathbf{n} \times [(\mathbf{p}_0 + \mathbf{T}_2) \times \mathbf{n}]] + \frac{1}{v_d}[\mathbf{m}_1 \times \mathbf{n}] \\ & + \frac{ik_d}{6}[\mathbf{n} \times [\mathbf{n} \times (\hat{Q}_1 + \hat{Q}_3)\mathbf{n}]] + \frac{ik_d}{2v_d}[\mathbf{n} \times \hat{M}_2\mathbf{n}] \\ & + \frac{k_d^2}{6}[\mathbf{n} \times [\mathbf{n} \times \hat{O}_2^{(e)}\mathbf{nn}]] + \frac{k_d^2}{6v_d}[\mathbf{n} \times \hat{O}_3^{(m)}\mathbf{nn}] \\ & - \frac{ik_d^3}{24}[\mathbf{n} \times [\mathbf{n} \times \hat{S}_3^{(e)}\mathbf{nnn}]]\Bigg). \end{aligned} \tag{34}$$

The total scattered power, defined as

$$P_{\text{sca}} = \frac{1}{2}\sqrt{\frac{\varepsilon_0\varepsilon_d}{\mu_0}}\int_\Omega |\mathbf{E}_\mathbf{n}(\mathbf{r})|^2 r^2 d\Omega, \tag{35}$$

where Ω is the total solid angle around the scatterer, can be written as

$$\begin{aligned} P_{\text{sca}} \simeq {} & \frac{k_0^4}{12\pi\varepsilon_0^2 v_d\mu_0}|\mathbf{p}_0 + \mathbf{T}_2|^2 + \frac{k_0^4\varepsilon_d}{12\pi\varepsilon_0 v_d}|\mathbf{m}|^2 \\ & + \frac{k_0^6\varepsilon_d}{1440\pi\varepsilon_0^2 v_d\mu_0}\sum_{\alpha\beta}|Q_{1\,\alpha\beta} + Q_{3\,\alpha\beta}|^2 \\ & + \frac{k_0^6\varepsilon_d^2}{160\pi\varepsilon_0 v_d}\sum_{\alpha\beta}|M_{2\,\alpha\beta}|^2 \\ & + \frac{k_0^8\varepsilon_d^2}{3780\pi\varepsilon_0^2 v_d\mu_0}\sum_{\alpha\beta\gamma}|O_{2\,\alpha\beta\gamma}^{(e)}|^2 \\ & + \frac{k_0^8\varepsilon_d^3}{3780\pi\varepsilon_0 v_d}\sum_{\alpha\beta\gamma}|O_{3\,\alpha\beta\gamma}^{(m)}|^2 \\ & + \frac{k_0^{10}\varepsilon_d^3}{145152\pi\varepsilon_0^2 v_d\mu_0}\sum_{\alpha\beta\gamma\tau}|S_{3\,\alpha\beta\gamma\tau}^{(e)}|^2. \end{aligned} \tag{36}$$

In the above expression, $\mathbf{p}_0 + \mathbf{T}_2$ is the exact electric dipole moment, $\mathbf{m}_1$ is the exact magnetic dipole moment, $\hat{Q}_1 + \hat{Q}_3$ is the exact electric quadrupole tensor, $\hat{M}_2$ is the exact magnetic quadrupole tensor, and $\hat{O}_3^{(m)}$ is the exact magnetic octupole tensor in the spherical multipole decomposition. The same expressions for low-order exact multipoles were obtained in

Refs. [16,17] using another approach. Additional contributions to the electric octupole term $\hat{O}_2^{(e)}$ and the electric 16-pole term $\hat{S}_3^{(e)}$ can be found considering the next terms of $\mathbf{S}_l$ from Eq. (7).

It was shown in Ref. [16] that the LWA multipole moments can be obtained from the exact multipole moments using a small argument approximation of the Bessel functions in expressions (21)–(29).

III. DIRECTIONAL SCATTERING

One can expect that with the derived exact multipole moments more accurate results for light scattering compared to the LWA approach can always be obtained [16], especially if the scatterer size is large compared to the wavelength. For example, the electric field of the scattered wave along an arbitrary vector $\mathbf{n}$ (directional scattering) calculated using Eq. (34) with several first-multipole contributions could be more accurate than that obtained using LWA equation (5) with the same number of multipoles. However, in general this statement is not true. As mentioned above, the Taylor expansion with LWA multipoles is convergent and can be applied, similar to the spherical harmonic series, for multipole decomposition of the scattered field by any finite-size object. Moreover, we show below that in several important cases, the LWA multipole moments produce more accurate results than that obtained with the exact multipole moments of the same order. An important example is the directional scattering of light by shape-anisotropic objects with different geometrical dimensions like finite-size plates, disks, rings, rods, etc.

First, we turn to the discussion of exponential factor $\exp[-ik_d(\mathbf{n}\cdot\mathbf{r}')]$ in Eq. (4). For a fixed direction of scattering $\mathbf{n}$, the exponential factor can be rewritten as $\exp(-ik_d r'_\parallel)$, where $r'_\parallel = r'\cos\gamma$ is the projection of vector $\mathbf{r}'$ on $\mathbf{n}$. Thus, in contrast to the conditions $k_d r' \ll 1$ (where all $\mathbf{r}'$ are from V_s) and $D \ll \lambda$ (where D is the biggest dimension of the scatterer), we get a weaker condition for the application of LWA equation (5),

$$k_d r'_\parallel = k_d r'\cos\gamma \ll 1 \quad \forall\, r' \in V_s, \tag{37}$$

where the maximum $r'_\parallel$ is equal to the projection $D_\parallel$ of the biggest scatterer dimension on $\mathbf{n}$. This means that for directional scattering LWA can be applied when

$$D_\parallel \ll \lambda. \tag{38}$$

However, in practical cases it is possible that the size parameters

$$k_d D_\parallel \ll 1 \lesssim k_d D \tag{39}$$

for particles with anisotropic shapes, characterized by large size differences in different space directions.

Let us assume that condition (39) is satisfied for directional scattering along $\mathbf{n}$. Then, $\exp[-ik_d(\mathbf{n}\cdot\mathbf{r}')] \approx 1$ in Eq. (4), and the scattered electric field is determined by

$$\mathbf{E}_\mathbf{n}(\mathbf{r}) \simeq \frac{k_0^2 e^{ik_d r}}{4\pi\varepsilon_0 r}[\mathbf{n}\times[\mathbf{p}\times\mathbf{n}]], \tag{40}$$

where

$$\mathbf{p} = \frac{i}{\omega}\int_{V_s}\mathbf{j}(\mathbf{r}')d\mathbf{r}' \tag{41}$$

is the LWA (ordinary) electric dipole moment. It is important that Eq. (40) cannot be derived from the general expression (34) with the exact multipole moments since the size parameter $k_d D \gtrsim 1$ is not small, so that the small argument expansion of the Bessel functions in Eqs. (21)–(29) cannot be formally applied. In this case, one has to use Eq. (34) with *all* exact multipole moments.

For $k_d D_\parallel \ll 1$ and $k_d D_\parallel \sim \cos\gamma \ll 1$ resulting in the approximation of the Legendre polynomials $P_l(\cos\gamma) \simeq P_l(0)$, the exact expression for the electric field, Eq. (7), can be approximated by

$$\mathbf{E}_\mathbf{n}(\mathbf{r}) \simeq i\omega\mu_0\frac{e^{ik_d r}}{4\pi r}(\hat{U}-\mathbf{nn}) \times\sum_{l=0}^{\infty}(-i)^l(2l+1)P_l(0)\int_{V_s}j_l(k_d r')\mathbf{j}(\mathbf{r}')d\mathbf{r}', \tag{42}$$

where $\mathbf{p}$ following from Eq. (40) is given by

$$\mathbf{p} = \frac{i}{\omega}\sum_{l=0}^{\infty}(-i)^l(2l+1)P_l(0)\int_{V_s}j_l(k_d r')\mathbf{j}(\mathbf{r}')d\mathbf{r}'. \tag{43}$$

Comparing Eqs. (41) and (43), we get the identity

$$\sum_{l=0}^{\infty}(-i)^l(2l+1)j_l(k_d r')P_l(0) \equiv 1, \tag{44}$$

where $P_l(0) = 0$ for odd l and $P_l(0) \neq 0$ for even l, for example, $P_0(0) = 1$, $P_2(0) = -1/2$, $P_4(0) = 3/8$, $P_6(0) = -5/16$, $P_8(0) = 35/128$, $P_{10}(0) = -63/256$, … Importantly, the identity (44) is independent of the parameter $k_d r'$. This means that an infinite number of terms with even $l = 0, 2, 4, 6, 8, \ldots$ has to be taken into account in the sum in order to get the exact value of 1. Only in the case when $k_d r' = 0$ are all spherical Bessel functions with $l > 0$ equal to zero, except $j_0(0) = 1$; therefore, only the term with $l = 0$ survives in (44). If $k_d r' \neq 0$, Eq. (44) can be approximated by a finite N number of terms:

$$C_N(k_d r') = \sum_{l=0}^{N}(-i)^l(2l+1)j_l(k_d r')P_l(0) \approx 1, \tag{45}$$

where N depends on the magnitude of $k_d r'$ and the required approximation accuracy. For a fixed value of $k_d r'$, subsequent terms starting from a relatively large l (depending on the $k_d r'$ value) provide very small corrections because of negligibly small values of the corresponding spherical Bessel functions (see Fig. 1). For example, if $k_d r' = 5$, we get from Eq. (45)

$$C_0(5) = -0.1918, \quad C_2(5) = 0.1450, \quad C_4(5) = 0.7762,$$
$$C_6(5) = 0.9711, \quad C_8(5) = 0.9978, \quad C_{10}(5) = 0.9999.$$

We see that in this case at least six terms (up to $l = 10$) are required to provide a good approximation for Eq. (44). Note that, if instead of r', the biggest scatterer size D is used in Eq. (45), it allows one to estimate the maximum

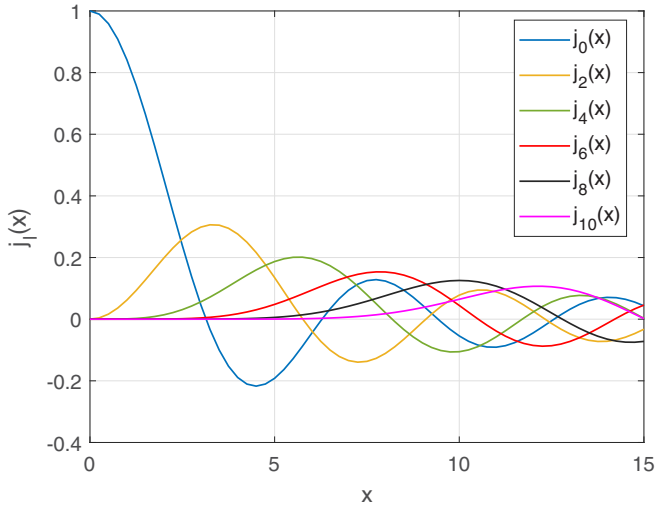

FIG. 1. Spherical Bessel functions.

number and order of exact multipoles for accurate calculations of the scattered electric field in a certain direction and the total scattering cross section. Note that the contributions of exact multipole moments with $l \gg k_d D$ in the exact multipole decompositions are negligibly small. There exists a simple approximation of the spherical Bessel functions $j_l(x)$ in the region of small arguments $x \to 0$ [23]:

$$j_l(x \to 0) \sim \frac{x^l}{1 \times 3 \times 5 \times \cdots \times (2l+1)}. \tag{46}$$

This approximation can also be used for estimates of spherical Bessel functions if the condition $x \ll l$ is fulfilled.

It is not possible to make a direct transition between expressions of the exact multipole moments (21)–(29) and the LWA multipole moments in the case of directional scattering when $k_d D_\parallel \ll 1 \lesssim k_d D$. In this case, the scattered electric field (40) is determined by only the LWA electric dipole term (41), whereas many exact multipole contributions will be required to get the same accuracy (43). The effective number of the required exact multipole moments depends on the biggest scatterer size D and increases with the increasing $k_d D$, approaching infinity when $k_d D \to \infty$. This means that if D is equal to infinity, for example, in the case of an infinite cylindrical rod, the presented exact multipole decomposition is not applicable. This also follows from the fact that for infinite rods the condition $r \gg D$ for the observation point cannot be satisfied.

The electric dipole approximation (40) can be used for calculations of the scattered power in a finite solid angle $\Delta\Omega$,

$$\begin{aligned} P(\Delta\Omega) &= \frac{1}{2}\sqrt{\frac{\varepsilon_0\varepsilon_d}{\mu_0}}\int_{\Delta\Omega}|\mathbf{E}_\mathbf{n}|^2 r^2 d\Omega \\ &\approx \frac{k_0^4}{32\pi^2\varepsilon_0^2}\sqrt{\frac{\varepsilon_0\varepsilon_d}{\mu_0}}\int_{\Delta\Omega}(|\mathbf{p}|^2 - |\mathbf{n}\cdot\mathbf{p}|^2)d\Omega, \end{aligned} \tag{47}$$

if for any $\mathbf{n}$ from $\Delta\Omega$ the maximal scatterer size projection $D_\parallel^\mathbf{n}$ on the direction $\mathbf{n}$ satisfies the conditions $D_\parallel^\mathbf{n} \ll \lambda$. Note that contributions of the exact multipole moments with odd numbers l will be significantly suppressed.

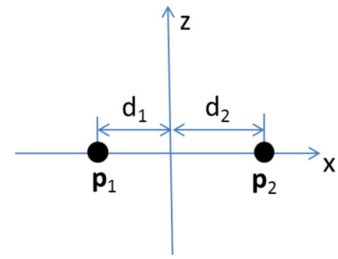

FIG. 2. Physical model including two electric dipoles with moments $\mathbf{p}_1$ and $\mathbf{p}_2$ located in air.

In the following section we provide a few examples related to some "paradoxes" with applications of exact multipoles.

IV. DEMONSTRATIVE EXAMPLES

Let us consider a simple system of two oscillating electric point dipoles located in air at $\mathbf{r}_1 = (-d_1, 0, 0)$ and $\mathbf{r}_2 = (d_2, 0, 0)$, as shown in Fig. 2. Total polarization $\mathbf{P}$ (or the electric current density $\mathbf{j}$) of this system can be written as

$$\mathbf{P}(\mathbf{r}) = \frac{i}{\omega}\mathbf{j}(\mathbf{r}) = \mathbf{p}_1\delta(\mathbf{r}-\mathbf{r}_1) + \mathbf{p}_2\delta(\mathbf{r}-\mathbf{r}_2). \tag{48}$$

Here we assume that dipoles oscillate with the same frequency ω. Inserting the current density from Eq. (48) into Eq. (4) and taking into account that the unit vector $\hat{z}$ is perpendicular to $\mathbf{r}_1$ and $\mathbf{r}_2$, the electric field radiated along the z axis is

$$\mathbf{E}_{\hat{z}}(z) = \frac{k_0^2 e^{ik_d r}}{4\pi\varepsilon_0 z}(\hat{U} - \hat{z}\hat{z})\mathbf{p} \equiv \frac{k_0^2 e^{ik_d r}}{4\pi\varepsilon_0 z}\mathbf{p}_\perp, \tag{49}$$

where $\mathbf{p} = \mathbf{p}_1 + \mathbf{p}_2$ is the total LWA electric dipole moment and $\mathbf{p}_\perp = \mathbf{p}_{1\perp} + \mathbf{p}_{2\perp}$ is its projection on the xy plane. Equation (49) is exact and does not depend on the distance between the dipoles.

If in this system we consider the electric field $\mathbf{E}'_{\hat{z}}(z)$ generated by the exact electric dipole moment $\mathbf{p}_0 + \mathbf{T}_2$, we obtain

$$\mathbf{E}'_{\hat{z}}(z) = \frac{k_0^2 e^{ik_d r}}{4\pi\varepsilon_0 z}(\hat{U} - \hat{z}\hat{z})(\mathbf{p}_0 + \mathbf{T}_2). \tag{50}$$

Using Eqs. (21) and (25), we have

$$\mathbf{p}_0 = j_0(k_0 d_1)\mathbf{p}_1 + j_0(k_0 d_2)\mathbf{p}_2, \tag{51}$$

$$\begin{aligned} \mathbf{T}_2 = \frac{k_0^2}{2}\Bigg\{ &\frac{j_2(k_0 d_1)}{(k_0 d_1)^2}[3(\mathbf{r}_1\cdot\mathbf{p}_1)\mathbf{r}_1 - d_1^2\mathbf{p}_1] \\ &+ \frac{j_2(k_0 d_2)}{(k_0 d_2)^2}[3(\mathbf{r}_2\cdot\mathbf{p}_2)\mathbf{r}_2 - d_2^2\mathbf{p}_2]\Bigg\}, \end{aligned} \tag{52}$$

resulting in the radiated electric field

$$\begin{aligned} \mathbf{E}'_{\hat{z}}(z) = \frac{k_0^2 e^{ik_d r}}{4\pi\varepsilon_0 z}\{ &j_0(k_0 d_1)\mathbf{p}_{1\perp} + j_0(k_0 d_2)\mathbf{p}_{2\perp} \\ &+ \frac{j_2(k_0 d_1)}{2}[3(\hat{x}\cdot\mathbf{p}_1)\hat{x} - \mathbf{p}_{1\perp}] \\ &+ \frac{j_2(k_0 d_2)}{2}[3(\hat{x}\cdot\mathbf{p}_2)\hat{x} - \mathbf{p}_{2\perp}]\}, \end{aligned} \tag{53}$$

where $\hat{x}$ is the unit vector along the x axis. One can see that $\mathbf{E}'_{\hat{z}}(z)$ depends on the dipole positions and that $\mathbf{E}'_{\hat{z}}(z) \neq \mathbf{E}_{\hat{z}}(z)$.

Recall that $\mathbf{E}_{\hat{z}}(z)$ is the exact solution (49) and is independent of the distance between the dipoles. Thus, for accurate calculation of the radiated electric field using exact multipoles one has to take into account contributions of high-order multipole moments. LWA is much simpler and, with the single-dipole term, leads to the exact result. The last statement is true for any number of point dipoles arbitrarily located on a plane for radiation generated in the perpendicular (forward and backward) direction.

Another example is related to light scattering by a dielectric ring structure with parameters shown in Fig. 3(a). The dielectric constant of the ring structure is $\varepsilon_p = 16$, and the dielectric constant of the surrounding medium $\varepsilon_d = 1$. Using discrete dipole approximation (DDA) [24], we numerically calculate the distribution of the induced polarization $\mathbf{P}(\mathbf{r})$ inside the ring, then, using Eq. (1), the scattered electric field without any multipole decomposition, and, finally, angular distribution of the *total* scattered power $P^s(\varphi, \theta)$ in the far field:

$$P^s(\varphi,\theta) = \frac{1}{2}\sqrt{\frac{\varepsilon_0}{\mu_0}}[|E^s_\varphi(r,\varphi,\theta)|^2 + |E^s_\theta(r,\varphi,\theta)|^2]r^2, \quad (54)$$

where (r, φ, θ) are coordinates of the observation point in the spherical coordinate system: r is the radial coordinate, φ and θ are the azimuthal and polar angles, respectively; and E^s_φ and E^s_θ are angular components of the scattered electric field. A detail description and discussions of the DDA numerical method and its applicability for electromagnetic scattering problems are presented in Ref. [24]. Note that the DDA is equivalent to other calculation methods, such as the volume integral equation method and the digitized Green's function method [25,26].

We calculate the scattered electric field first without multipole decomposition directly from Eq. (4) and then using two multipole decompositions with the same number of multipole terms using LWA equation (5) and exact multipole equation (34). We also calculate angular distributions $P^s(\varphi, \theta)$ for $\varphi = 0$ and $\theta \in [0, \pi]$ ($\theta \in [0, 180^o]$) with and without multipole decomposition approaches. In multipole decompositions we take into account contributions of the LWA multipoles $\mathbf{p}$ [electric dipole (ED)], $\mathbf{m}$ [magnetic dipole (MD)], $\mathbf{T}$ [torodal dipole (TD)] , $\hat{Q}$ [electric quadrupole (EQ)], $\hat{M}$ [magnetic quadrupole (MQ)], and $\hat{O}$ [electric octupole (EOC)] [18] and with the same number of exact spherical multipoles $\mathbf{p}_0$, $\mathbf{m}_1$, $\mathbf{T}_2$, $\hat{Q}_1$, $\hat{M}_2$, $\hat{O}_2$. Calculated results are presented in Figs. 3(b) and 3(c) for two sets of the size parameters kD and $kD_{||}$ (where k is the wave number in air). Note that the $\theta = 0$ and $\theta = \pi$ cases correspond to forward and backward scattering. Comparing the red and green curves with the blue curve with triangles in Fig. 3(b), one can see that for $0 \leqslant \theta \leqslant 25^o$ and $155^o \leqslant \theta \leqslant 180^o$ the LWA multipole decomposition provides very good agreement with total numerical calculations (without multipole decomposition), whereas the approach with the exact multipoles provides poor results at these angles. For agreement with the total numerical result [the curve with blue triangles in Fig. 3(b)], calculations with exact multipoles need to involve higher-order terms up to $l \simeq 10$. As expected, for $25^o < \theta < 155^o$, corresponding to side scattering, the exact multipole approach gives better agreement with the total numerical calculations compared to

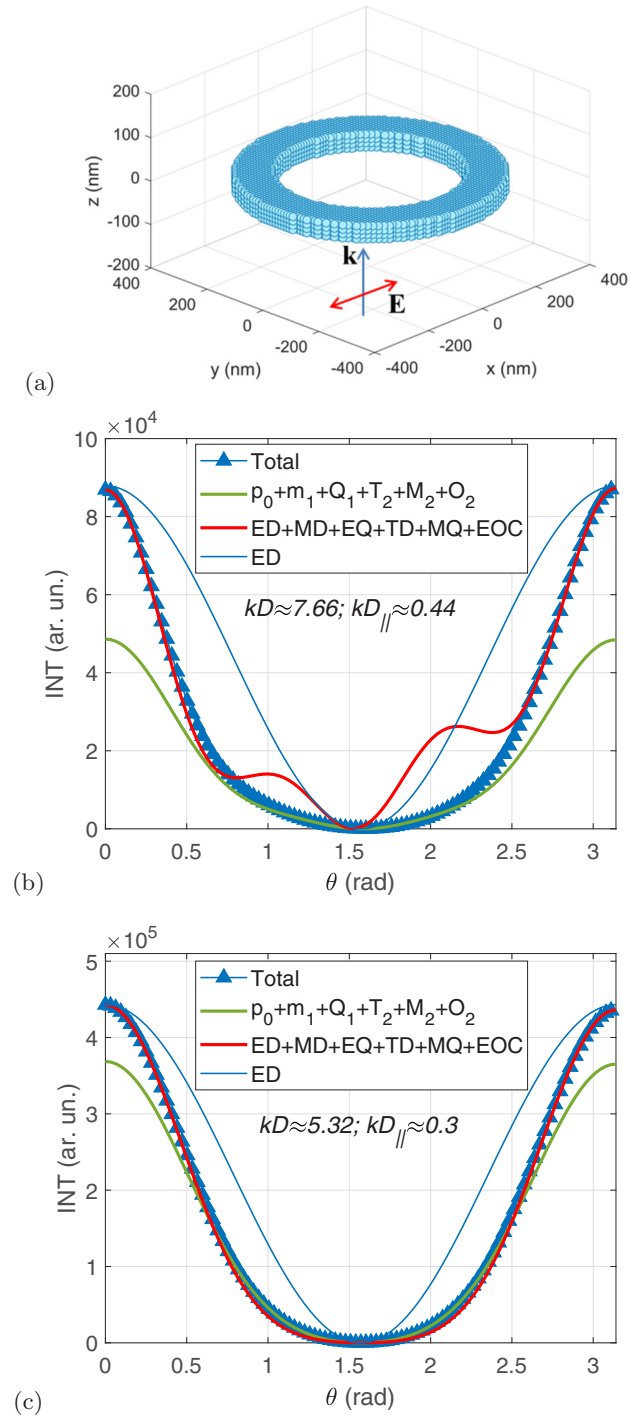

FIG. 3. (a) Scattering object: a dielectric ring located in air is irradiated by a plane light wave propagating along the z axis with linear polarization along the x axis. The geometrical parameters of the ring are external radius $R_{ext} = 350$ nm, internal radius $R_{in} = 250$ nm, and ring thickness $H = 40$ nm. (b) and (c) Angular distribution of the scattered power $P^s(\varphi, \theta)$ for $\varphi = 0$ and $\theta \in [0, \pi]$ calculated using the numerical method without multipole decomposition (the curve with blue triangles) and with multipole decompositions: the red curve corresponds to LWA with the indicated multipoles; the green curve is calculated using the indicated exact multipoles, and the blue ED curve corresponds to the LWA electric dipole contribution. kD and $kD_{||}$ are the size parameters defined in the main text.

LWA. In Figs. 3(b) and 3(c), one can also see that the forward ($\theta = 0$) and backward ($\theta = \pi$) scattering is determined by only the LWA electric dipole contribution given by ED curves. As expected, with growing wavelength [Fig. 3(c)], differences between LWA and exact multipole approaches are reduced. However, still, the LWA multipoles provide a better approximation for forward and backward scattering [the red and green curves in Fig. 3(c)].

The final example is related to light scattering by a dielectric finite-length rod with diameter and length determined in Fig. 4(a). We again consider angular distributions of the scattered power $P^s(\varphi, \theta)$ for $\varphi = 0$ and $\theta \in [0, \pi]$ ($\theta \in [0, 180^o]$) with and without multipole decomposition approaches. In Figs. 4(b) and 4(c) the size parameters satisfy the conditions $kD_{||} \ll 1 < kD$. Angular distributions of the scattered power calculated without multipole decomposition is presented by the curves with blue triangles in Figs. 4(b) and 4(c). A comparison of these curves with that calculated using multipole decompositions with different numbers of multipole terms allows us to demonstrate the accuracy of the applied multipole decompositions. One can see that the forward scattering ($\theta = 0$) and backward scattering ($\theta = \pi$) are determined by the only ED contribution in the LWA case [the dashed black curve in Fig. 4(b)]. In contrast, the exact multipole decomposition provides an accurate approximation for forward and backward scattering by taking into account contributions of multipoles up to the electric octupole O_2 and magnetic quadrupole M_2 [the red curve in Fig. 4(c)]. For arbitrary θ both multipole decompositions provide accurate approximations when the multipole moments up to the electric octupole and magnetic quadrupole are used in Figs. 4(b) and 4(c). Our simulations show that the above analysis is also valid for rods with larger diameters corresponding to the size parameter $kD_{||} \simeq 0.5$.

The presented examples demonstrate that calculations with a limited number of exact multipoles do not automatically provide better results than LWA. There exist scattering directions where LWA provides more accurate results.

V. CONCLUSION

Starting from a general expression for radiated (scattered) electric field obtained from Maxwell equations, the electric field multipole decomposition with exact multipole moments was derived in real space using the Cartesian coordinate representation. The obtained expressions are in agreement with previous publications [16,17], where derivations were made in momentum space. The developed approach was used to compare applications of the long-wavelength approximation and exact multipole moments for modeling directional light scattering by a shape-anisotropic finite-size scatterer with different geometrical dimensions. It was demonstrated that in certain cases the LWA approach requires fewer multipoles for modeling directional scattering. It was shown that the physical reason why the LWA approach works better than the exact spherical multipole decomposition is the presence of a small parameter providing better convergence of the Taylor expansion determining LWA multipoles. This parameter is the ratio between the biggest scatterer size projection in the light scattering direction and the light wavelength. If this

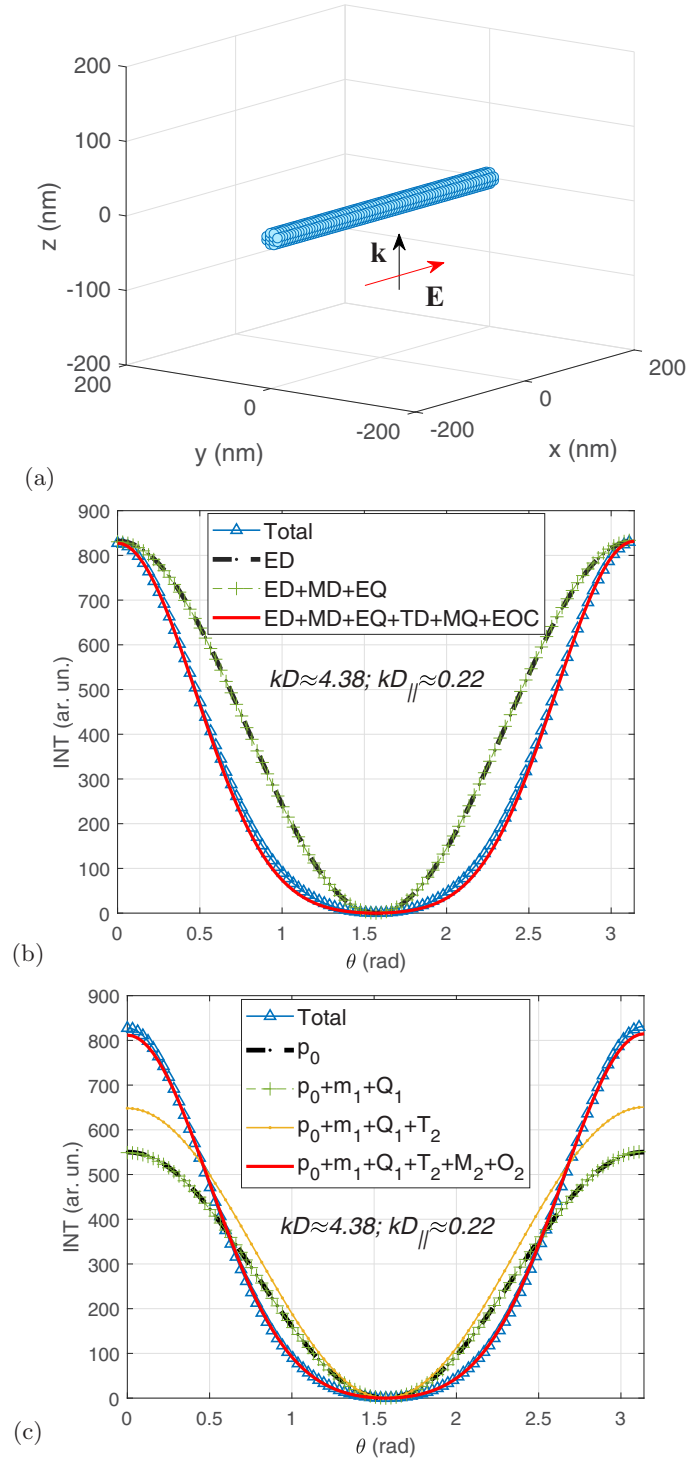

FIG. 4. (a) Scattering object: a dielectric rod located in air is irradiated by a plane light wave propagating along the z axis with linear polarization along the x axis. The geometrical parameters of the rod are a length of 400 nm and a diameter of 20 nm. (b) and (c) Angular distribution of the scattered power $P^s(\varphi, \theta)$ for $\varphi = 0$ and $\theta \in [0, \pi]$ calculated using the numerical method without multipole decomposition (the curves with blue triangles). (b) Results of LWA multipole decomposition with different numbers of multipole terms and (c) calculations with different numbers of exact multipoles. kD and $kD_{||}$ are the size parameters.

ratio is small ($\ll 1$) only low-order LWA multipoles determine the scattered field even in the case when the real scatterer sizes are larger than the light wavelength. However, the number of exact multipoles required for accurate approximation of the same directional scattered field can be significantly higher. Detailed explanations of this seeming paradox were given.

ACKNOWLEDGMENTS

The authors acknowledge financial support from the Deutsche Forschungsgemeinschaft (DFG, German Research Foundation) under Germany's Excellence Strategy within the Cluster of Excellence PhoenixD (EXC 2122, Project No. 390833453).

[1] J. D. Jackson, *Classical Electrodynamics* (Wiley, New York, 1999).

[2] L. D. Landau and E. M. Lifshitz, *The Classical Theory of Fields* (Pergamon, New York, 1971).

[3] R. E. Raab and O. L. De Lange, *Multipole Theory in Electromagnetism: Classical, Quantum, and Symmetry Aspects, with Applications* (Oxford University Press, Oxford, 2005).

[4] E. E. Radescu and G. Vaman, Exact calculation of the angular momentum loss, recoil force, and radiation intensity for an arbitrary source in terms of electric, magnetic, and toroid multipoles, Phys. Rev. E **65**, 046609 (2002).

[5] J. Chen, J. Ng, Z. Lin, and C. T. Chan, Optical pulling force, Nat. Photon. **5**, 531 (2011).

[6] A. B. Evlyukhin, C. Reinhardt, and B. N. Chichkov, Multipole light scattering by nonspherical nanoparticles in the discrete dipole approximation, Phys. Rev. B **84**, 235429 (2011).

[7] P. D. Terekhov, K. V. Baryshnikova, Y. A. Artemyev, A. Karabchevsky, A. S. Shalin, and A. B. Evlyukhin, Multipolar response of nonspherical silicon nanoparticles in the visible and near-infrared spectral ranges, Phys. Rev. B **96**, 035443 (2017).

[8] A. B. Evlyukhin and S. I. Bozhevolnyi, Resonant unidirectional and elastic scattering of surface plasmon polaritons by high refractive index dielectric nanoparticles, Phys. Rev. B **92**, 245419 (2015).

[9] V. M. Dubovik and V. V. Tugushev, Toroid moment in electrodynamics and solid-state physics, Phys. Rep. **187**, 145 (1990).

[10] N. A. Nemkov, A. A. Basharin, and V. A. Fedotov, Electromagnetic sources beyond common multipoles, Phys. Rev. A **98**, 023858 (2018).

[11] D. C. Zografopoulos, J. F. Algorri, A. Ferraro, B. García-Cámara, J. M. Sánchez-Pena, and R. Beccherelli, Toroidal metasurface resonances in microwave waveguides, Sci. Rep. **9**, 7544 (2019).

[12] E. A. Gurvitz, K. S. Ladutenko, P. A. Dergachev, A. B. Evlyukhin, A. E. Miroshnichenko, and A. S. Shalin, The high-order toroidal moments and anapole states in all-dielectric photonics, Laser Photonics Rev. **13**, 1800266 (2019).

[13] P. Grahn, A. Shevchenko, and M. Kaivola, Electromagnetic multipole theory for optical nanomaterials, New J. Phys. **14**, 093033 (2012).

[14] C. F. Bohren and D. R. Huffman, *Absorption and Scattering of Light by Small Particles* (Wiley, New York, 2008).

[15] R. Alaee, C. Rockstuhl, and I. Fernandez-Corbaton, Exact multipolar decompositions with applications in nanophotonics, Adv. Optical Mater. **7**, 1800783 (2018).

[16] R. Alaee, C. Rockstuhl, and I. Fernandez-Corbaton, An electromagnetic multipole expansion beyond the long-wavelength approximation, Opt. Commun. **407**, 17 (2018).

[17] I. Fernandez-Corbaton, S. Nanz, R. Alaee, and C. Rockstuhl, Exact dipolar moments of a localized electric current distribution, Opt. Express **23**, 33044 (2015).

[18] A. B. Evlyukhin, T. Fischer, C. Reinhardt, and B. N. Chichkov, Optical theorem and multipole scattering of light by arbitrarily shaped nanoparticles, Phys. Rev. B **94**, 205434 (2016).

[19] L. Novotny and B. Hecht, *Principles of Nano-optics* (Cambridge University Press, New York, 2006).

[20] O. Keller, Local fields in the electrodynamics of mesoscopic media, Phys. Rep. **268**, 85 (1996).

[21] A. B. Evlyukhin, C. Reinhardt, E. Evlyukhin, and B. N. Chichkov, Multipole analysis of light scattering by arbitrary-shaped nanoparticles on a plane surface, J. Opt. Soc. Am. B **30**, 2589 (2013).

[22] Legendre polynomials, https://en.wikipedia.org/wiki/Legendre_polynomials.

[23] D. A. Hill, *Electromagnetic Fields in Cavities: Deterministic and Statistical Theories* (Wiley, Hoboken, NJ, 2009).

[24] M. A. Yurkin and A. G. Hoekstra, The discrete dipole approximation: An overview and recent developments, J. Quant. Spectrosc. Radiat. Transfer **106**, 558 (2007).

[25] A. Lakhtakia, Strong and weak forms of the method of moments and the coupled dipole method for scattering of time-harmonic electromagnetic-fields, Int. J. Mod. Phys. C **03**, 583 (1992),

[26] F. M. Kahnert, Numerical methods in electromagnetic scattering theory, J. Quant. Spectrosc. Radiat. Transfer **79–80**, 775 (2003).